Microscopic Nanomechanical Dissipation in Gallium Arsenide Resonators

M. Hamoumi,[1] P. E. Allain,[1] W. Hease,[1] E. Gil-Santos,[1] L. Morgenroth,[2] B. Gérard,[3] A. Lemaître,[4] G. Leo,[1] and I. Favero[1]

[1]*Matériaux et Phénomènes Quantiques, Université Paris Diderot, CNRS UMR 7162, Sorbonne Paris Cité, 75013 Paris, France*

[2]*Institut d'Electronique, de Microélectronique et de Nanotechnologie, UMR CNRS 8520, Avenue Poincaré, 59652, Villeneuve d'Ascq, France*

[3]*III-V Lab, 1 Avenue Augustin Fresnel, 91767 Palaiseau, France*

[4]*Centre de Nanosciences et de Nanotechnologies, CNRS, Université Paris Sud, Université Paris-Saclay, C2N-Marcoussis, Route de Nozay, 91460 Marcoussis, France*

(Received 17 January 2018; revised manuscript received 16 March 2018; published 29 May 2018)

We report on a systematic study of nanomechanical dissipation in high-frequency (≈300 MHz) gallium arsenide optomechanical disk resonators, in conditions where clamping and fluidic losses are negligible. Phonon-phonon interactions are shown to contribute with a loss background fading away at cryogenic temperatures (3 K). Atomic layer deposition of alumina at the surface modifies the quality factor of resonators, pointing towards the importance of surface dissipation. The temperature evolution is accurately fitted by two-level systems models, showing that nanomechanical dissipation in gallium arsenide resonators directly connects to their microscopic properties. Two-level systems, notably at surfaces, appear to rule the damping and fluctuations of such high-quality crystalline nanomechanical devices, at all temperatures from 3 to 300 K.

DOI: 10.1103/PhysRevLett.120.223601

The physical origin of nanomechanical dissipation is a topic of curiosity and debate, motivated by a vast number of applications. Ultralow-dissipation nanomechanical resonators represent a key ingredient for optomechanics, which investigates the interaction of light and mechanical motion [1,2]. They are becoming crucial in weak-force resolution [3,4], mass sensing [5–8], and mesoscopic quantum operations such as ground-state cooling of mechanical motion [9,10] and entanglement between mechanical systems [11]. For example, gallium arsenide (GaAs) nano-optomechanical disk resonators, whose high-frequency radial breathing modes (RBMs) strongly couple to optical whispering gallery modes (WGMs) [12,13], are expected to display low mechanical dissipation thanks to their constitutive crystalline epitaxial material, and they have indeed achieved large Q-frequency products. However, despite the achieved control of clamping losses [14,15], their ultimate mechanical performances are still affected by residual damping processes. The investigation of these processes is the focus of the present work.

In this Letter, specific dissipation channels are made negligible by experimental conditions (vacuum operation that suppresses fluidic damping) or by design (pedestal engineering that suppresses anchoring losses [14,15]), enabling a direct analysis of intrinsic loss mechanisms. These are investigated by comparative measurement of identical resonators made out of two distinct epitaxial wafers, and accurately compared to models of phonon-phonon damping. Surface nanomechanical dissipation is investigated by observing the influence of an atomic layer deposition (ALD) of alumina onto the resonators. The temperature dependence between 3 and 300 K is systematically measured and fitted by two-level systems (TLS) models, allowing the emergence of a microscopic picture of damping processes in GaAs resonators. Our results indicate that TLS dissipation dominates at all temperatures, despite the crystalline nature of the material. By comparing distinct wafers, as well as pristine and surface-treated resonators, we provide evidence about the nature and localization of TLS. Our study finally provides a consistent picture of noise mechanisms affecting high-Q crystalline nanomechanical systems, which are generally regarded as the best candidates for quantum applications.

The employed GaAs optomechanical disks have a radius of 5.5 μm, are 200 nm thick, and sit on a 1.8-μm-high aluminium gallium arsenide (AlGaAs) pedestal of radius 500 nm. The samples are fabricated from two distinct wafers (1 and 2) grown by molecular beam epitaxy (MBE) under distinct conditions but with the same nominal structure: 200 nm$(GaAs)/1.8$ μm$(Al_{0.8}Ga_{0.2}As)/500$ μm (semi-insulating GaAs). The disk and their optical coupling suspended waveguides [16] are first patterned in a negative resist using electron beam lithography. The resist is developed and serves as a mask during the inductively coupled plasma reactive ion etching (ICP-RIE) with a $SiCl_4/Ar$ chemistry. The pedestal is underetched with a hydrofluoric acid solution, and the waveguide inverted taper endings are freed using a BCK solution [17].

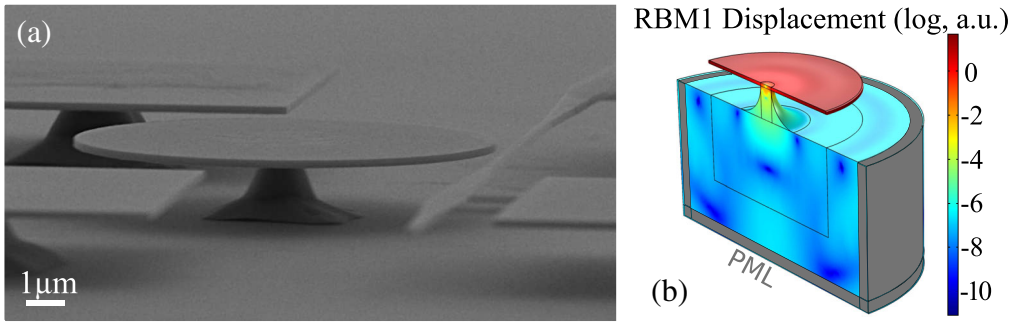

FIG. 1. (a) A 200-nm-thick GaAs disk resting on a 500-nm-radius AlGaAs pedestal. The suspended optical coupling waveguide with inverted tapers can be seen on the right side. The square-shaped pads on the link hold the guide of the adjacent device (not shown). (b) FEM simulation of the first-order RBM of the disk. The color scale corresponds to the modulus of the displacement vector, in logarithm scale and in arbitrary units. The black lines correspond to the different geometrical domains at rest for the FEM simulation. Perfectly matched layers (PMLs) are introduced at the substrate boundaries. The displacement is strongly localized within the disk, corresponding to a clamping $\Gamma_m < 2.5$ kHz ($Q_m > 6.5 \times 10^5$).

Figure 1(a) shows an electron micrograph of a fabricated device.

In the following, we invariably measure the quality factor Q_m of a mechanical mode or its energy dissipation rate $\Gamma_m = \omega_m/Q_m$, obtained from the full width at half maximum of the corresponding resonance if the frequency noise is negligible, which is the case here (not shown). The mechanical spectrum is measured optomechanically by tuning the laser on the flank of a WGM resonance and analyzing the radio-frequency noise of the output light [12]. To avoid dynamical optomechanical backaction modifying Γ_m [1,2], the measurements are taken as a function of optical power and the linear evolution extrapolated at zero power. We focus here on the first-order RBM, which has a frequency of $f_m = \omega_m/2\pi = 260$ MHz and is only subject to intrinsic dissipation channels. Indeed, GaAs disk resonators are operated in a cryostat (accessible range 2.6 to 300 K) and under vacuum ($\lesssim 10^{-5}$ mbar). At such pressure, the gas damping of the breathing motion is negligible [7,18]. The dimensions of the disk and pedestal are also chosen to render clamping losses negligible. The latter are simulated numerically by the finite element method (FEM), as shown in Fig. 1(b), and our previous work in the clamping-limited regime showed good agreement with experiments [14,15]. We adopt here a disk geometry for which our tolerance on pedestal dimensions bounds clamping losses Γ_m to below 3.26 kHz, corresponding to a $Q_m > 5 \times 10^5$. In what follows, this channel of dissipation can be neglected, whatever the temperature.

The measurements of Γ_m between 3 and 300 K are shown in Fig. 2(a) for nominally identical resonators fabricated with the exact same process, but out of the two distinct epitaxial wafers (1 and 2). These results reveal two obvious features. First, the intrinsic dissipation tends to increase with temperature, in a similar manner for the two wafers; second, the dissipation is larger in wafer 1 than in wafer 2. The temperature evolution of Γ_m distinguishes three regimes: (1) a slow increase between 3 K and 150 K; (2) a peak around 180 K; and (3) a quasiplateau from 200 K to 300 K. The similar behavior of wafers 1 and 2 points towards some universality, whose origin remains to be elucidated. Fluidic and clamping losses being negligible, the dissipation processes must take place in the bulk or at the surface of resonators.

We first analyze the mechanical dissipation induced by interaction of the 260 MHz (mechanical) phonon with high-frequency ($\simeq h/k_B T$) thermal phonons. This phonon-phonon damping was discussed in the bulk, using the Landau-Rumer approach (valid when $\omega_m \tau_{\rm ph} \gg 1$) or a Boltzmann equation approach like that employed by Akhiezer (valid when $\omega_m \tau_{\rm ph} \ll 1$), where $\tau_{\rm ph}$ is a relaxation time for thermal phonons. The relation between these approaches was discussed by Maris [19]. The Boltzmann equation description assumes thermal phonons to be localized with respect to the mechanical wavelength, a condition implying that $k_B T \gg h f_m$, which is satisfied here where $T > 3$ K. Upon incidence of a mechanical wave (even spatially uniform), the population of thermal phonons is perturbed as a consequence of the lattice anharmonicity and dissipates energy via collisions to return to equilibrium. A collision time approximation can be adopted, provided $\omega_m \tau_{\rm ph} < 1$, leading to an expression of this Akhiezer damping [19–22]:

$$\Gamma_m = \omega_m \frac{C_p T (\Delta\gamma)^2}{\rho \bar{c}^2} \frac{\omega_m \tau_{\rm ph}}{1 + (\omega_m \tau_{\rm ph})^2}, \qquad (1)$$

where C_p and ρ are the volume specific heat and density, $(\Delta\gamma)^2$ is the variance of the Grüneisen parameter over thermal phonons involved in the process, and $3/\bar{c}^3 = 1/c_l^3 + 2/c_t^3$ is the mean Debye sound velocity, with c_l (c_t) being the longitudinal (transverse) velocity. The

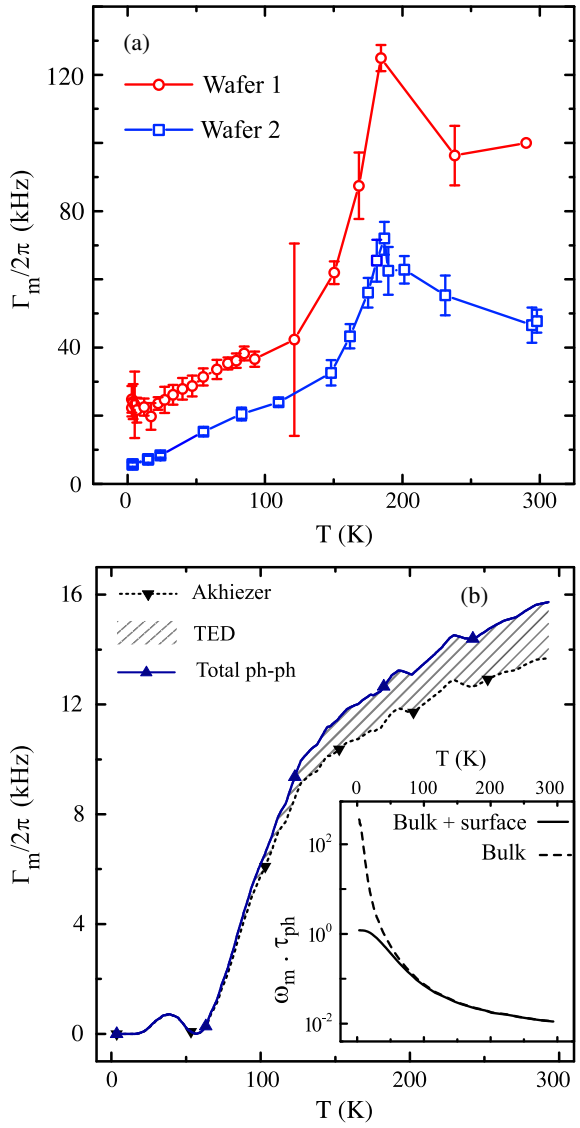

FIG. 2. (a) Measured mechanical dissipation rate as a function of temperature. The two wafers were grown in two distinct MBE chambers. Fifty resonators were measured in total, and the results shown here are representative. (b) Modeled mechanical dissipation due to phonon-phonon interactions, for both Akhiezer and TED mechanisms. Note that the damping cancels artificially around 60 K with the Grüneisen parameter, as a result of our approximation on $\Delta\gamma$ (see text). Inset: Temperature evolution of the parameter $\omega_m\tau_{\mathrm{ph}}$ (see text).

relaxation of thermal phonons occurs both in the bulk and at the resonator's surface $\tau_{\mathrm{ph}}^{-1} = \tau_{\mathrm{bulk}}^{-1} + \tau_{\mathrm{surf}}^{-1}$, where $\tau_{\mathrm{bulk}} = 3\kappa/C_p\bar{c}^2$ is a temperature-dependent relaxation time [22], with κ being the bulk thermal conductivity and τ_{surf} being a surface relaxation time governed by the resonator geometry. In the spirit of prior works on micro- and nanoscale resonators [23,24], we adopt the relation $\tau_{\mathrm{surf}} = \sqrt[3]{V_R}/\bar{c}$, with V_R being the resonator's volume. The temperature dependance of τ_{ph} is mainly set by κ and C_p [25], and in the second order by $\bar{c}$ [26], leading to the evolution of $\omega_m\tau_{\mathrm{ph}}$ shown in the inset of Fig. 2(b). The Akhiezer mechanism requires a finite variance of the Grüneisen parameter $\Delta\gamma \neq 0$, which is approximated [27] by $(\Delta\gamma)^2 = 1.5\bar{\gamma}^2$, with $\bar{\gamma}$ being the average Grüneisen parameter and the factor 1.5 taken to reproduce bulk acoustic attenuation around 300 MHz [27]. The Akhiezer prediction of Eq. (1) is reported in Fig. 2(b) and accounts for the first part of the phonon-phonon damping. The strain field of the RBM being nonuniform, the anharmonicity of the lattice ($\bar{\gamma} \neq 0$) additionally induces temperature gradients within the vibrating resonator, leading to irreversible heat flows and dissipation. This thermoelastic damping (TED) [21,24,28–30] can be simulated by FEM, resulting in the extra contribution reported in Fig. 2(b) when the temperature dependence of thermal expansion is accounted for [31]. The total phonon-phonon damping is finally plotted in Fig. 2(b). It shows an overall increase with temperature, yet with no peak at 180 K or plateau. Whatever the temperature, its amplitude is also smaller than in measurements, being essentially negligible for $T < 50$ K and representing a small contribution at higher temperatures. Our models hence indicate that phonon-phonon mechanisms do not govern the dissipation of our nanomechanical resonators. This conclusion is supported by the clear difference in dissipation amplitude between the two wafers shown in Fig. 2(a), which points towards material-related effects that need to be elucidated.

In order to investigate the contribution of surfaces, we deposit a 6.5 nm layer of alumina by ALD onto resonators made out of wafer 2, and compare in Fig. 3(a) the temperature dependence of dissipation before and after ALD treatment. The ALD treatment increases the dissipation at all temperatures: the peak around 180 K vanishes, and the plateaulike behavior is replaced by a monotonic increase. The outcome of this trial is that surfaces play an important role in the mechanical dissipation of GaAs nanoresonators. This will be further illustrated in the analysis below.

Indeed, the exact temperature dependance of Γ_m, together with its variation with the employed surface treatment or wafer, can help in identifying the microscopic origin of dissipation. With this mindset, we systematically analyze our results with TLS models initially developed for amorphous materials [32–35]. These models depict microscopic defects and configurations as potential energy double wells [Fig. 3(b)] with the following parameters: the asymmetry Δ, the barrier height V_0, or the well-to-well tunneling amplitude $\Delta_0 \approx 2E_0/\pi \exp[-d(mV_0/2\hbar^2)^{1/2}]$, with d being the separation between wells and E_0 the ground-state energy of a single well [32–35]. For a TLS distribution $P(\Delta, \Delta_0)$, the dissipation rate is in general given by [32]

$$\Gamma_m = \omega_m \frac{2\eta^2 N_{\mathrm{TLS}}}{\rho c_s^2 k_B T} \iint_{\mathbb{R}+} d\Delta d\Delta_0 \frac{\Delta^2}{E^2} \mathrm{sech}^2\left(\frac{E}{2k_B T}\right) \times \frac{\omega_m \tau}{1 + (\omega_m \tau)^2} P(\Delta, \Delta_0), \quad (2)$$

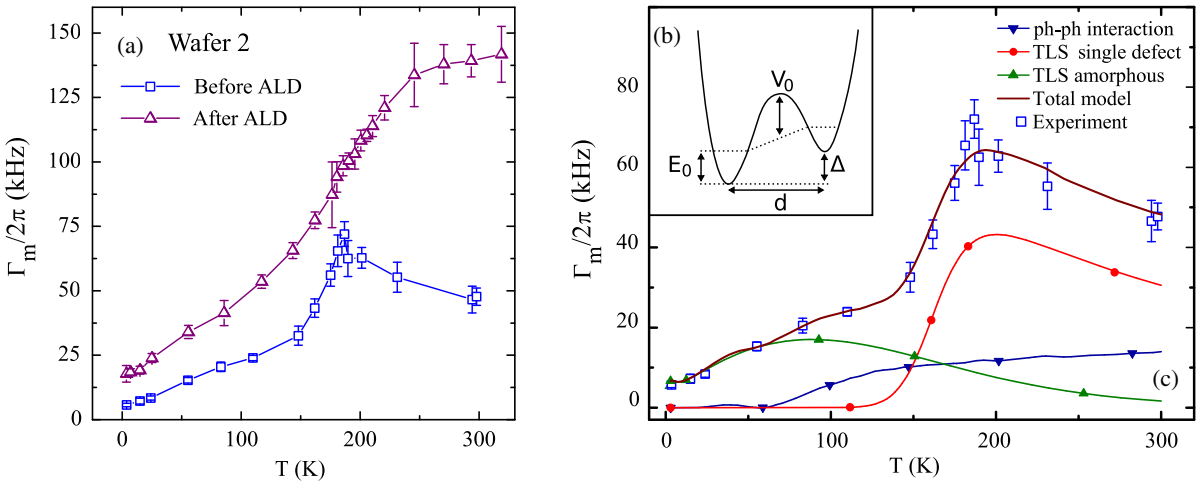

FIG. 3. (a) Intrinsic mechanical dissipation before and after ALD of 6.5 nm of Al_2O_3. (b) Double-well model for TLS. (c) Modeling of the intrinsic mechanical dissipation in wafer 2 using phonon-phonon interactions and TLS models.

with η being the deformation potential coupling of a TLS to the mechanical phonon (in eV), N_{TLS} the density of TLS, ρ and c_s the density and sound velocity of the material, $E = \sqrt{E_0^2 + \Delta^2}$, and τ the TLS relaxation time. For $T \geq 10$ K, several energy levels of the wells are typically populated. In this so-called *thermally activated regime*, the relaxation time is given by a quasi-Arrhenius law $\tau = \tau_0 e^{(V_0/k_B T)} sech([\Delta/2k_B T])$, where τ_0^{-1} is of the order of the Debye frequency of the material [34], and $\Delta \approx E$, leading a simplified expression of the dissipation [35], where a distribution $P(\Delta, V_0)$ is used equivalently.

In order to fit the measured temperature-dependent dissipation, we consider two distinct distributions introduced in the literature [35,36] and sum up their contribution using the linearity of Eq. (2): (1) The *single-defect distribution* $P(\Delta', \Delta_0') = \delta(\Delta' - \Delta) \cdot \delta(\Delta_0' - \Delta_0)$ considers both Δ and Δ_0, and hence E, as fixed, with δ being the Dirac function. This distribution assumes a single type of TLS, and makes use of an alternative deformation potential $D = (\Delta/E)\eta$ for conciseness. (2) The *amorphous distribution* $P(\Delta, V_0) = f(\Delta) \cdot g(V_0)$, where f is a Gaussian function and g a quasi-Gaussian function, with mean value 0 and width Δ_1 and V_1 [35]. This model is typically used for amorphous materials where a broad distribution of TLS couples to acoustic waves. In Fig. 3(c), these two contributions sum up with the prior phonon-phonon contribution to reproduce the mechanical dissipation measured on resonators of wafer 2 in the range $T \geq 10$ K, with TLS parameters shown in Table I. We note that the dissipation below 10 K is difficult to model using the thermally activated regime, such that the two lowest temperature points are fitted with a coherent version of the relaxation time [32,37], $\tau^{-1} = (\eta^2 \Delta_0^2 E/2\pi\rho c_s^5 \hbar^4) \coth([E/2k_B T])$. The obtained level of agreement sheds light on the microscopic nature of dissipation. The mechanical damping up to 100 K is well explained by an amorphous TLS model, which suggests a role of the surface reconstruction layer, whose amorphous nature was observed by transmission electron microscopy [38]. In order to model the dissipation at higher T, the single-defect model must, however, be used on top. The related defect has an activation energy of ≈0.1 eV, which is in the range of known deep centers in

TABLE I. Fitting parameters for TLS models in the thermally activated regime. The mathematical rigidity of the fitting function allows unequivocal parameter estimation, with error intervals corresponding to a factor-2 reduction of the distance between model and data.

	Wafer 2 (before ALD)		Wafer 2 (after ALD)		Wafer 1 (before ALD)	
	Amorphous	Single defect	Amorphous	Single defect	Amorphous	Single defect
Δ_1/k_B (K)	$1430_{\pm 400}$	⋯	$1400_{\pm 200}$	⋯	$1200_{\pm 300}$	⋯
V_1/k_B (K)	$1020_{\pm 250}$	⋯	$1300_{\pm 200}$	⋯	$1000_{\pm 350}$	⋯
τ_0 (s)	$1.76^{+3.24}_{-1.26} \times 10^{-13}$	$3.8^{+0.4}_{-0.9} \times 10^{-12}$	$2.57^{+2}_{-1} \times 10^{-13}$	$4.2^{+0.7}_{-0.5} \times 10^{-10}$	$2.7^{+2.3}_{-2.2} \times 10^{-13}$	$4.36_{\pm 1} \times 10^{-12}$
E (meV)	⋯	$100_{\pm 5}$	⋯	50^{+3}_{-1}	⋯	$100_{\pm 4}$
$\eta^2 N_{\mathrm{TLS}}$ (eV^2 m^{-3})	$6.05_{\pm 0.5} \times 10^{25}$	⋯	$1.49_{\pm 0.15} \times 10^{26}$	⋯	$1.04_{\pm 0.2} \times 10^{26}$	⋯
$D^2 N_{\mathrm{TLS}}$ (eV^2 m^{-3})	⋯	$1.24^{+0.1}_{-0.3} \times 10^{27}$	⋯	$7.59_{\pm 0.5} \times 10^{25}$	⋯	$2.34_{\pm 0.4} \times 10^{27}$

GaAs [39]. For a deformation potential ≈10 eV, the inferred density of TLS is $\approx 10^{18}$–10^{19} cm^{-3}, well above the unintentional doping of our epitaxial GaAs (10^{14} cm^{-3} range), suggesting the formation of TLS at the surfaces in a density superior to the bulk. If all TLS are on surfaces, a surface density of $\approx 10^{13}$–10^{14} cm^{-2} can be deduced, which is precisely the range of surface-state densities reported on intrinsic GaAs surfaces [40]. The localization of TLS can further be investigated by looking at resonators that are ALD-treated or fabricated out of wafer 1 (see Table I). The ALD treatment modifies both the amorphous and single-defect distributions, indicating again that both types of TLS are present at surfaces. It enhances the density of amorphous TLS, which is consistent with the amorphous nature of deposited alumina, but it decreases the density of single-defect TLS, which is reminiscent of surface passivation by ALD [41]. The superior mechanical dissipation in wafer 1 compared to 2 appears to originate from a different density of amorphous TLS, which is again consistent with their localization at surfaces, since surface absorption of photonic resonators fabricated out of wafer 1 was also observed to be superior to that of wafer 2 [41].

In summary, we have reported a systematic study of intrinsic nanomechanical dissipation in GaAs resonators. Microscopic models indicate that two-level systems dominate damping at any temperature between 3 and 300 K. While in conflict with the common sense that crystalline devices are less affected by TLS than their amorphous counterparts [42,43], this conclusion is consistent with the presence of an amorphous reconstruction layer at their surface. Such a layer already rules the optical dissipation of high-Q GaAs resonators with a large surface-to-volume ratio [38], and we bring here a series of evidence that TLS impacting their nanomechanical dissipation are mainly localized at surfaces as well. Our models anticipate that freezing these fluctuating TLS would be beneficial, predicting a mechanical quality factor Q_m beyond 10^9 at 10 mK. The related Q-frequency product $Q_m \times f_m$, which is an important figure of merit in the quantum domain [2,14], would reach the 10^{17}–10^{18} range for GaAs resonators, equaling the performances of other crystalline devices in quartz [44] and silicon [45]. Ultralow-temperature experiments, possibly below the millikelvin level, may ultimately reveal how far the performances of nanomechanics can be pushed, for metrological and quantum applications.

This work was supported by the European Research Council (ERC) through the Ganoms Project (No. 306664). The authors thank Bernard Perrin and Eddy Collin for fruitful comments.

[1] I. Favero and K. Karrai, Nat. Photonics **3**, 201 (2009).
[2] M. Aspelmeyer, T. J. Kippenberg, and F. Marquardt, Rev. Mod. Phys. **86**, 1391 (2014).
[3] H. Miao, K. Srinivasan, and V. Aksyuk, New J. Phys. **14**, 075015 (2012).
[4] A. G. Krause, M. Winger, T. D. Blasius, Q. Lin, and O. Painter, Nat. Photonics **6**, 768 (2012).
[5] J. Tamayo, P. M. Kosaka, J. J. Ruz, Á. San Paulo, and M. Calleja, Chem. Soc. Rev. **42**, 1287 (2013).
[6] F. Liu, S. Alaie, Z. Leseman, and M. Hossein-Zadeh, Opt. Express **21**, 19555 (2013).
[7] E. Gil-Santos, C. Baker, D. T. Nguyen, A. Lemaître, C. Gomez, S. Ducci, G. Leo, and I. Favero, Nat. Nanotechnol. **10**, 810 (2015).
[8] E. Gil-Santos, C. Baker, D. T. Nguyen, W. Hease, C. Gomez, A. Lemaître, S. Ducci, G. Leo, and I. Favero, in *Proceedings of the 29th International Conference on Micro Electro Mechanical Systems (IEEE MEMS)* (IEEE, New York, 2016), pp. 238–241, DOI: 10.1109/MEMSYS.2016.7421603.
[9] J. Teufel, T. Donner, D. Li, J. Harlow, M. Allman, K. Cicak, A. Sirois, J. D. Whittaker, K. Lehnert, and R. W. Simmonds, Nature (London) **475**, 359 (2011).
[10] R. W. Peterson, T. P. Purdy, N. S. Kampel, R. W. Andrews, P.-L. Yu, K. W. Lehnert, and C. A. Regal, Phys. Rev. Lett. **116**, 063601 (2016).
[11] K. Børkje, A. Nunnenkamp, and S. M. Girvin, Phys. Rev. Lett. **107**, 123601 (2011).
[12] J. C. L. Ding, C. Baker, A. Andronico, D. Parrain, P. Senellart, A. Lemaître, S. Ducci, G. Leo, and I. Favero, Gallium arsenide disk optomechanical resonators, in *Handbook of Optical Microcavities* (Pan Stanford, Singapore, 2014), p. 381.
[13] I. Favero, Gallium arsenide disks as optomechanical resonators, in *Cavity Optomechanics* (Springer, New York, 2014), pp. 149–156, DOI: 10.1007/978-3-642-55312-7_7.
[14] D. T. Nguyen, C. Baker, W. Hease, S. Sejil, P. Senellart, A. Lemaitre, S. Ducci, G. Leo, and I. Favero, Appl. Phys. Lett. **103**, 241112 (2013).
[15] D. T. Nguyen, W. Hease, C. Baker, E. Gil-Santos, P. Senellart, A. Lemaître, S. Ducci, G. Leo, and I. Favero, New J. Phys. **17**, 023016 (2015).
[16] C. Baker, C. Belacel, A. Andronico, P. Senellart, A. Lemaitre, E. Galopin, S. Ducci, G. Leo, and I. Favero, Appl. Phys. Lett. **99**, 151117 (2011).
[17] W. Hease, Gallium Arsenide Disk Optomechanical Resonators Approaching the Quantum Regime, Ph.D. thesis, Paris Diderot University, 2016.
[18] S. S. Verbridge, H. G. Craighead, and J. M. Parpia, Appl. Phys. Lett. **92**, 013112 (2008).
[19] H. J. Maris, Interaction of sound waves with thermal phonons in dielectric crystals, in *Physical Acoustics*, Vol. 8 (Academic Press, New York, 1971), pp. 279–345.
[20] H. Maris, Phys. Rev. **175**, 1077 (1968).
[21] B. Perrin, Phys. Rev. B **24**, 6104 (1981).
[22] A. Cleland, *Foundations of Nanomechanics* (Springer, New York, 2003).
[23] W. Fon, K. C. Schwab, J. M. Worlock, and M. L. Roukes, Phys. Rev. B **66**, 045302 (2002).
[24] K. Kunal and N. R. Aluru, Phys. Rev. B **84**, 245450 (2011).
[25] J. Blakemore, J. Appl. Phys. **53**, R123 (1982).
[26] R. Cottam and G. Saunders, J. Phys. C **6**, 2105 (1973).

[27] R. Cottam and G. Saunders, J. Phys. C **7**, 2447 (1974).
[28] G. Zener, Phys. Rev. **53**, 90 (1938).
[29] R. Lifshitz and M. L. Roukes, Phys. Rev. B **61**, 5600 (2000).
[30] A. A. Kiselev and G. J. Iafrate, Phys. Rev. B **77**, 205436 (2008).
[31] T. Soma and K. Kudo, J. Phys. Soc. Jpn. **48**, 115 (1980).
[32] W. A. Phillips, Rep. Prog. Phys. **50**, 1657 (1987).
[33] D. Tielburger, R. Merz, R. Ehrenfels, and S. Hunklinger, Phys. Rev. B **45**, 2750 (1992).
[34] S. Rau, C. Enss, S. Hunklinger, P. Neu, and A. Würger, Phys. Rev. B **52**, 7179 (1995).
[35] R. Vacher, E. Courtens, and M. Foret, Phys. Rev. B **72**, 214205 (2005).
[36] S. Hunklinger and W. Arnold, Ultrasonic properties of glasses at low temperatures, in *Physical Acoustics*, Vol. 12 (Academic Press, New York, 1976), pp. 155–215, DOI: 10.1016/B978-0-12-477912-9.50008-4.
[37] W. A. Phillips, Phys. Rev. Lett. **61**, 2632 (1988).
[38] D. Parrain, C. Baker, G. Wang, B. Guha, E. Gil Santos, A. Lemaître, P. Senellart, G. Leo, S. Ducci, and I. Favero, Opt. Express **23**, 19656 (2015).
[39] K. Yamanaka, S. Naritsuka, K. Kanamoto, M. Mihara, and M. Ishii, J. Appl. Phys. **61**, 5062 (1987).
[40] S. D. Offsey, J. M. Woodall, A. C. Warren, P. D. Kirchner, T. I. Chappell, and G. D. Pettit, Appl. Phys. Lett. **48**, 475 (1986).
[41] B. Guha, F. Marsault, F. Cadiz, L. Morgenroth, V. Ulin, V. Berkovitz, A. Lemaître, C. Gomez, A. Amo, S. Combrié *et al.*, Optica **4**, 218 (2017).
[42] T. S. Faust, J. Rieger, M. J. Seitner, J. P. Kotthaus, and E. M. Weig, Phys. Rev. B **89**, 100102 (2014).
[43] L. G. Villanueva and S. Schmid, Phys. Rev. Lett. **113**, 227201 (2014).
[44] M. Goryachev, D. L. Creedon, E. N. Ivanov, S. Galliou, R. Bourquin, and M. Tobar, Appl. Phys. Lett. **100**, 243504 (2012).
[45] S. M. Meenehan, J. D. Cohen, G. S. MacCabe, F. Marsili, M. D. Shaw, and O. Painter, Phys. Rev. X **5**, 041002 (2015).